Materials Advances

ROYAL SOCIETY OF CHEMISTRY

PAPER

View Article Online
View Journal

Cite this: DOI: 10.1039/d6ma00307a

Density functional theory prediction of a novel hybrid organic–inorganic bidentate perovskite with charge transport perpendicular to the inorganic layer

Sergio Romero-García, [a] Susana Ramos-Terrón, †[b] Gustavo de Miguel, [b] Per Hyldgaard, [c] Luis Camacho [b] and David López-Durán *[a]

Bidentate perovskites, a novel family within this class of solids, have recently attracted the attention of the scientific community. Their spacers feature a dual anchoring mechanism onto the inorganic framework, characteristic of the Dion-Jacobson phases, while the attachment occurs within the same octahedral layer, as observed in the Ruddlesden–Popper perovskites. In this work, we present a hybrid organic–inorganic bidentate perovskite that exhibits diamines as organic spacers between the inorganic layers of PbI_6 octahedra, in particular, 4,4′-dithiodianiline. A geometric optimization was carried out within the Density Functional Theory framework as implemented in the Quantum Espresso code. We employed the nonempirical consistent-exchange vdW-DF-cx functional [DOI:10.1103/PhysRevB.51.4014] to obtain precise geometry and electronic properties. The total density of states, band structure, valence and conduction band, and changes in the electronic clouds are analysed, finding that the band gap of this new perovskite is 2.55 eV, which reveals a semiconductor nature. In the valence band, the dominant contribution originates from the inorganic layer, whereas in the conduction band the initial contributions arise from the spacer, in particular, from the carbon and sulfur atoms. This suggests charge transport between the inorganic layers, perpendicularly and through the organic moieties. Our findings therefore contribute to the development of novel materials for optoelectronic applications, such as solar cells.

Received 5th March 2026,
Accepted 9th April 2026

DOI: 10.1039/d6ma00307a

rsc.li/materials-advances

1. Introduction

Hybrid organic–inorganic perovskites (HOIPs) are a family of semiconductors that adopt the perovskite-derived ABX_3 structure, in which the A-site is an organic cation (ammonium, for instance), the B-site a divalent metal (most commonly Pb^{2+} or Sn^{2+}), and X a halide anion, enabling extensive compositional freedom without abandoning the same basic lattice motif.[1] The exceptional suitability of HOIPs for photovoltaic applications arises from their combination of strong visible-light absorption, broad tunability and low-cost manufacturing routes, which together enable high power conversion efficiencies in thin-film solar cells.[2] The field's rapid uptake was catalysed by the demonstration that organometal halide perovskites can operate as efficient photoabsorbers in solar devices,[3] and by subsequent evidence that solution-processed HOIPs can support long carrier transport lengths compatible with high collection efficiencies.[4,5] At the microscopic level, first-principles studies have associated the impressive optoelectronic performance with the changes in the orientation of the organic molecule with respect to the inorganic frame.[6]

However, HOIPs exhibit several drawbacks that must be addressed to enable long-term use. The very hybrid bonding and ionic sublattice that confer facile processing and compositional tunability also introduce vulnerabilities: HOIPs devices can undergo chemical and environmental degradation pathways involving moisture and oxygen, thermal stress and photo-induced reactions.[7] HOIPs also exhibit significant ion migration under electric fields and illumination, a process that can induce current–voltage hysteresis and limit operational stability in devices.[8] In this context, the exploration of alternative structural motifs within the HOIPs family, including novel geometric

[a] Departamento de Física, Universidad de Córdoba, Campus de Rabanales, Edificio Albert Einstein (C-2), Ctra. Nnal. IV-A, km. 396, Córdoba, Spain. E-mail: dlduran@uco.es
[b] Departamento de Química Física y Termodinámica Aplicada, Instituto Químico para la Energía y el Medio Ambiente, IQUEMA, Universidad de Córdoba, Campus de Rabanales, Edificio Marie Curie (C-3), C, tra. Nnal. IV-A, km. 396, Córdoba, Spain
[c] Department of Microtechnology and Nanoscience, MC2, Chalmers University of Technology, SE-41296 Göteborg, Sweden
† Present address: Semiconductor Materials for Sustainability Laboratory, Institute of Materials Science of Seville and Department of Condensed Matter Physics, University of Seville – Spanish National Research Council (US–CSIC), Calle Américo Vespucio 49, Seville 41092, Spain.

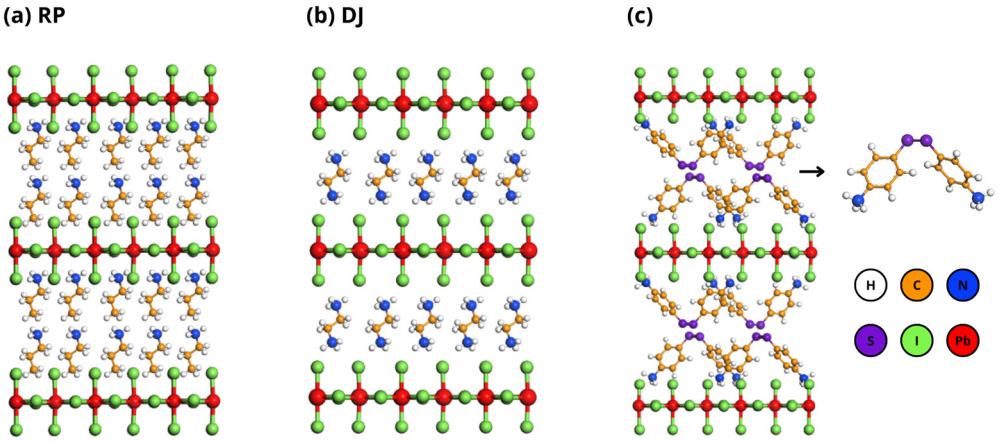

Fig. 1 Ruddlesden–Popper ($A'_2A_{n-1}B_nX_{3n+1}$) and Dion-Jacobson ($A''A_{n-1}B_nX_{3n+1}$) perovskites, panels (a) and (b), respectively. A is an organic or inorganic cation, B is a divalent metal (*i.e.*, Sn or Pb), X is a halogen anion (*i.e.*, I or Br) and n is an integer (n = 1, 2, 3...). In these plots A′ is the propylammonium for the case of the RP perovskites, panel (a), while for the DJ phase A″ is the ethylenediammonium, panel (b). The perovskite form proposed here uses 4,4′-dithiodianiline molecules as spacers, panel (c). In all cases n = 1.

arrangements and dimensionalities of the organic and inorganic sublattices, has emerged as a promising strategy to mitigate these limitations while preserving the favourable optoelectronic properties of the perovskite framework.

Among 2D perovskites, two main structural families are distinguished: Ruddlesden–Popper (RP) and Dion-Jacobson (DJ). The RP perovskites follow the general formula $A'_2A_{n-1}B_nX_{3n+1}$ where A′ is a monoammonium organic spacer, A is an organic or inorganic cation, B is a divalent metal (*i.e.*, Sn or Pb), X is a halogen anion (*i.e.*, I or Br) and n is an integer (n = 1, 2, 3...). The general formula for the DJ phase is $A''A_{n-1}B_nX_{3n+1}$, where in this case A″ is a diammonium organic spacer and the rest of the symbols have the same meaning. Both RP and DJ structures are shown in Fig. 1, in which n = 1. The inorganic part of the perovskites, that is, the slab formed by BX_6 octahedra, is a rigid structure due to the covalent nature of its bonds and can be considered as a layer. However, the 2D arrangement of organic molecules is no longer rigid, as these are connected by electrostatic interactions, which are weaker (*e.g.*, ion–ion, ion–dipole and atom–atom bridges). Furthermore, the number of spacer planes is determined by their protonation state. RP perovskites require two spacer planes, as they feature only one protonated terminal group (propylammonium in Fig. 1(a)). In contrast, DJ phases achieve equivalent octahedral interlayer connectivity with a single spacer plane, owing to the protonation of both terminal groups (ethylenediammonium in Fig. 1(b)). The geometric constraints imposed by these layered structures severely restrict the types and sizes of organic spacers that can be incorporated. This poses a challenge: introducing functional groups that modulate the semiconductor properties of the material in a controlled manner while preserving the crystal structure.[9]

Beyond the well-established RP and DJ families, recent work has demonstrated the emergence of a distinct class of two-dimensional metal halide perovskites based on intralayer bidentate coordination,[10–12] giving rise to bidentate perovskites. They exhibit a fundamentally different geometry in which a single organic ligand binds two adjacent metal sites within the same inorganic layer. In this way, rigid diammonium ligands were rationally designed to realise this intralayer bidentate motif, yielding structurally well-defined bidentate phase perovskites. They markedly enhance thermal robustness, stronger ligand–lattice binding energies, and substantially improved operational stability and photovoltaic performance compared with analogous RP and DJ systems.[11] Building on this advance, the subsequent perspective[12] contextualises the bidentate phase as a new structural paradigm in layered perovskites, highlighting its ability to overcome the conventional performance–stability trade-off by improved lattice matching and defect passivation, while outlining its broader implications for molecular design strategies and future extensions to higher-order multidentate architectures and lead-free compositions.

In this work, we propose a novel family of bidentate perovskites employing diamines as organic spacers, like in the DJ perovskites, but arranged in two molecular planes, as in the RP phase, with B = Pb and X = I (see Fig. 1(c)). Under this design, both ammonium groups of the diamine are oriented toward the same inorganic layer of octahedra, as illustrated in Fig. 1(c). Notably, the present approach enables the incorporation of bulkier spacers, thereby expanding the range of functionalization strategies available for tuning the optoelectronic properties of the resulting materials. The selected organic spacer is the 4,4′-dithiodianiline (DD, $[C_{12}H_{14}N_2S_2]^{2+}$, Fig. 1(c)), whose peculiar geometry, particularly the C–S–S–C dihedral angle, plays a key role because it aligns both terminal amine groups in the same direction. In what follows, and for clarity, this novel perovskite, with stoichiometry PbI_4DD (n = 1), will be denoted as ''PbI4DD''.

Having selected the spacer, we performed a theoretical characterization of structural details as well as electronic properties for the PbI4DD perovskite within the framework of Density functional theory (DFT).[13,14] We rely exclusively on robust, non-empirical, general-purpose exchange–correlation (XC) functional approximations, each with a high degree of documented transferability. This is necessary because the PbI4DD structure is new, incompletely characterized and we want our theoretical study to partly take the form of predictions that may subsequently be

experimentally tested. We have obtained the geometry, the density of states (DOS), the band structure (BS), the valence and conduction bands (VB, CB), and the changes in the electronic clouds in the consistent-exchange vdW-DF-cx version[15] of the vdW density functional (vdW-DF) method[16–18] for truly nonlocal-correlation DFT studies.

The paper is organized as follows: Sections 2 and 3 include the physical aspects and the theoretical and numerical details of the system under study, respectively. Results and discussion are presented in Section 4, while conclusions and perspectives for future work can be found in Section 5.

2. Overview of the physical aspects

2.1 Structural criteria for the selection of organic spacers in RP and DJ perovskites

To rationally design layered perovskite structures, it is essential to understand the structural constraints that govern the incorporation of organic spacers. These criteria are particularly relevant for RP and DJ perovskites, where the arrangement and size of the spacer play a key role in determining the stability and electronic behaviour of the material.

Fig. 2(a) shows the different views of a RP phase with a protonated amine, where propylammonium is used as an example. Regardless of whether the perovskite is RP or DJ, the organic spacers must fit into the surface area available between the octahedra of BX_6.

Two requirements, therefore, must be met by these spacers: (a) have a projected section less than or equal to the surface S, and (b) a suitable location of the ammonium group along the axis of the molecule, Fig. 2(b). The octahedra of the inorganic structure can be partially distorted to adapt to the peculiarities of the spacer's geometries, although this fact does not modify the surface area available to the spacer, Fig. 2(c). Moreover, the flexible nature of certain organic molecules could enable adequate coupling with these requisites. Numerous organic spacers have been reported in the literature that adapt to the above requirements.[19–27]

Structures with bulky organic spacers have been described, with a projected section greater than S and a stoichiometry of A'_2MX_4 or $A''MX_4$, as for RP and DJ with $n = 1$, respectively. However, in these cases, the 2D structure of the inorganic lattice breaks, forming 1D structures with the same stoichiometry.[20,28–31]

Moreover, monoammonium or diammonium organic presenting a projected section larger than S can be anchored on the inorganic layer by electrostatic interactions, covering partially the surface of adjacent octahedra. For these structures with bulky organic anchors, the organic material does not act as a spacer between layers of inorganic material, but by coating as a protective layer of the 3D perovskite nanostructures. These structures have been designated in the literature as quasi-2D RP or DJ perovskites, although they do not have adequate RP or DJ stoichiometry.[9,32–37]

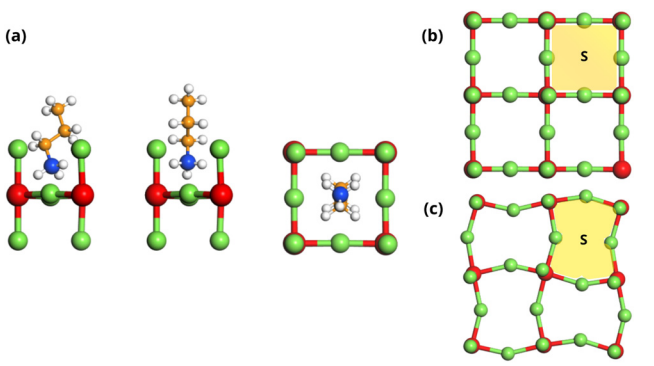

Fig. 2 Lateral and zenithal views of an Ruddlesden–Popper perovskite based on propylammonium, panel (a), with the available surface shown in panel (b). That area is the same even if the geometry is partially distorted, panel (c). Colour code as in Fig. 1.

2.2 Structural criteria for the selection of the DD spacer in the mixed RP/DJ perovskite

In this article, we propose the formation of a 2D perovskite with a double anchorage. Therefore, as an organic diammonium spacer is used, the stoichiometry of the formed structure must be identical to that of a DJ perovskite, even though the organic spacer is anchored only on one of the inorganic layers, as is the case in the RP phase, Fig. 3(a). Organic molecules suitable for this purpose must fulfil the following geometric requirements, see Fig. 3(a): (a) have a projected section less than or equal to the surface 2S, (b) both amino groups must be pointing in the same direction, and (c) in the case of $[PbI_6]^{4-}$, the distance between the amino groups should be between 5.9–6.3 Å, if the anchorage is over two gaps that share one side, or 8.4–8.9 Å, if the anchorage is between gaps that share only one vertex, with S of the order of 35–40 Å^2. These conditions considerably limit the type of spacer that can be used for this purpose, and we have selected DD, shown in Fig. 3(b). Once these requirements are fulfilled, the 3D crystal structure of DD can be constructed. Its characteristics were determined by X-ray crystallography, yielding a value of 80.2° for the C–S–S–C torsion angle and 8.9 Å for the N···N distance.[38] Let us remark, however, that the C–S–S–C angle shows some flexibility and it can be modified by both the protonation of the amino groups and the interaction with the inorganic octahedra, which have opposite charge. This inherent flexibility makes the DD spacer particularly suitable for accommodating the geometric constraints imposed by the inorganic framework. However, for this very reason, the number of possible initial configurations is large, and it is therefore necessary to ensure that the selected phase is stable (see details below).

To build the 2D perovskite using this spacer, we have started from a previous DJ structure, provided in the literature in which 4-aminomethylpiperidine (MP) is used as the spacer.[33] First, the crystal structure of this perovskite is transformed into P1 symmetry, then the four MP molecules that exist per unit cell are eliminated and a single DD molecule is introduced into the cell. The DD molecule is positioned so that its two nitrogen atoms occupy the same positions that the nitrogens of the ammonium groups of the removed MP molecules, approximately. In addition, the bisector of the torsion angle C–SS–C is located perpendicular to the inorganic layer, Fig. 3(b). The introduced DD molecule has the two nitrogens protonated and

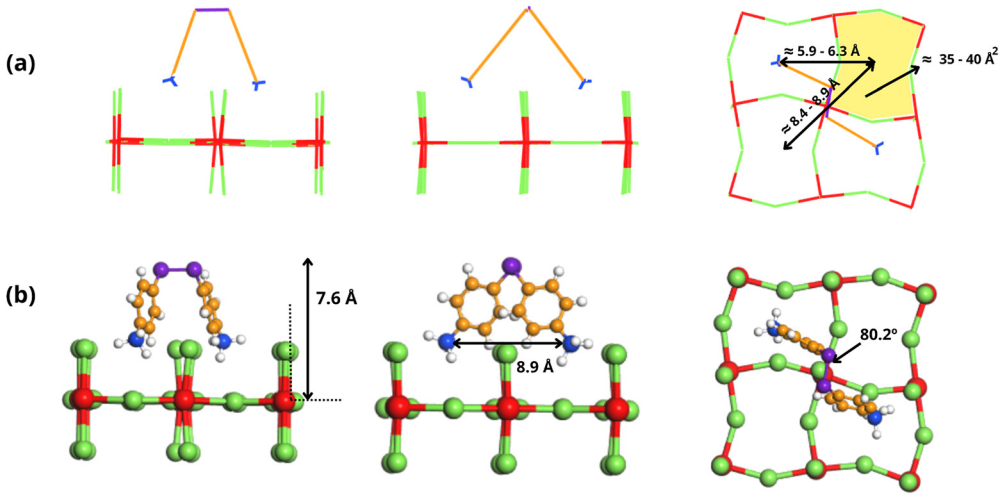

Fig. 3 Organic diammonium spacer in a DJ perovskite, together with the geometric requirements that must fulfil, panel (a). The particular case of a 4,4′-dithiodianiline molecule is shown in panel (b). Colour code as in Fig. 1.

a C–SS–C torsion angle of 80.2°. In the above structure, the distance between either of the two S atoms and the plane that defines the inorganic lattice is 7.6 Å. The crystal lattice is then expanded along perpendicularly to the inorganic layer by a distance 2 × (7.6 + 1.85) = 18.9 Å, where the value of 1.85 Å represents the vdW radius of sulfur. This expansion generates enough space to accommodate the remaining 3 DD molecules, necessary to compensate for the negative charge of the inorganic lattice. The methodology for introducing these three molecules is the same as that used with the first of them. The interaction between the inorganic slabs and the organic planes is fundamentally electrostatic in nature, involving ion–ion or ion–dipole interactions between the PbI_6 octahedra and the ammonium groups NH_3^+ (it should be remembered that the stoichiometry of the inorganic layer is actually $[PbI_4]^{2-}$, since 4 of the I atoms of the octahedron are shared by adjacent Pb atoms). This largely determines the relative positions of the DD molecule with respect to these slabs. Due to the relatively short distance between the sulfur atoms of two adjacent DD molecules and the strength of their interaction, S–S bridges should be considered as the next most important influence, with consequent effects on the relative positions between the spacers. Finally, N–H or N–Pb bridges would not play any relevant role, owing to the large separation between these atoms and/or the weakness of their interaction.

After this experience-based construction, a first and quick geometric optimization was carried out using the module CASTEP incorporated in the commercial software Biovia/Materials Studio.[39] The functional used was PBEsol[40] with TS dispersion correction.[41] Electron–ion interactions were described by ultrasoft pseudopotentials and the relativistic effects are incorporated by means of the Koelling-Harmon method. The structure obtained after this optimization is shown in Fig. 4(a). PBEsol calculations on closely-bonded oxide perovskites usually give geometric arrangements and relative stabilities in approximate agreement with experimental data, and the addition of a dispersion-correction[41–43] provides accuracy in structure predictions also to HOIPs.[44–47]

DD molecules have previously been used experimentally in the formation of a 2D perovskite, albeit in a different context, where the two amine groups of the molecule were not protonated.[10] In these circumstances, the interactions between the amine groups and the inorganic layers are not electrostatic, as in our case, given the absence of positive charge in the DD molecules, but through chelates, probably formed through N–Pb bonds.

3. Discussion of the DFT theoretical and numerical details

DFT can today accurately predict ground state properties of systems with hundreds if not thousands of atoms, thanks primarily to long and systematic investments into developing the exchange–correlation (XC) functional approximations. For example, DFT using the constraint-based generalized gradient approximation (GGA),[50–57] formulated in the PBE or PBEsol functionals,[40,56] delivers a robust and generally accurate description of both individual molecules and many extended materials with strong bonding.[58,59]

In mixed systems, for example, the novel PbI4DD 2D HOIP, one generally needs to either supplement the PBE/PBEsol by a semi-empirical dispersion correction, *e.g.*, as in PBE + D3 or PBE + TS,[41–43] or use the vdW-DF method for truly nonlocal-correlation nonempirical DFT.[16–18] Here, for our DFT characterization of the suggested PbI4DD perovskite, we proceed with the vdW-DF-cx version (abbreviated CX),[15] which aligns the nonlocal-correlation energy term of this vdW-DF with the screening implied in the GGA-type starting point to seek a systematic GGA extension.[60–63] The CX has been documented as a general purpose functional and more versatile than PBE. At the same time, it is more accurate on the strongly-bonded bulk matter than PBE and it is able to predict both the internal structure and inter-molecular excitations in molecular crystals.[60] For our goal of discussing and predicting properties, robustness on atomic-structure predictions is valuable.

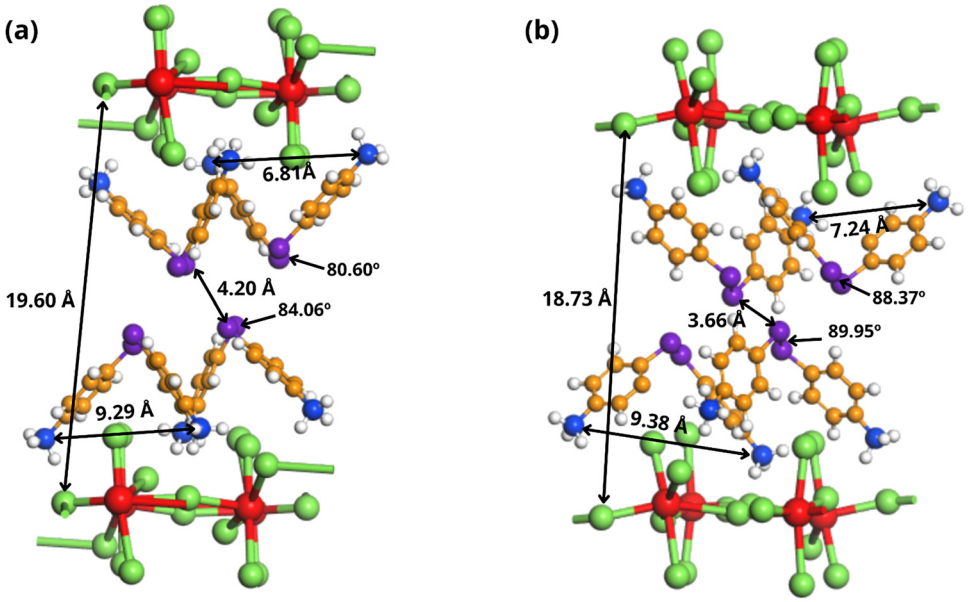

Fig. 4 Geometric optimization of the perovskite form proposed here, performed with the Biovia/Materials Studio[39] and Quantum Espresso[48,49] codes (panels (a) and (b), respectively). Colour code as in Fig. 1.

We face a new material and we cannot a priori know whether it is strongly bonded (in which case PBE may suffice) or whether the organic–inorganic binding requires use of the more versatile vdW-inclusive CX functional. Let us mention that as the CX functional has a GGA-type exchange its use in Kohn–Sham DFT leads to a well-understood underestimation of the predicted bandgap, like for the set of GGAs.

We have employed the Quantum Espresso (QE) suite of codes for planewave DFT and analysis[48,49] using norm-conserving pseudopotentials.[64] Our results, *i.e.*, predictions of geometric and electronic properties, for this new type of HOIP, have been obtained through a three-step procedure:

1. A CX geometric optimization whose starting point is the above-summarized dispersion-corrected PBEsol characterization. This initial prediction of both unit-cell and atomic structure implements relaxations defined by calculations of both forces and stresses and was completed at a 2175 eV (160 Ry) kinetic-energy cutoff (and 640 Ry for the charge-density representation) to leverage trust in accuracy, as documented in previous CX-based soft-matter structure optimizations.[62,65]

2. A self-consistent (scf) calculation followed by a non-self-consistent (nscf) calculation, achieving convergence with a kinetic-energy cutoff of 680 eV (50 Ry).

3. The extraction of the electronic features that we predict for our system using the QE post-processing tools.

The system was treated as non-spin-polarized and Brillouin zone sampling was performed employing the Monkhorst–Pack method,[66] with $4 \times 4 \times 4$ k-points for the CX geometric optimization as well as for the scf step and with $8 \times 8 \times 8$ k-points for the nscf step. The convergence thresholds in the structure optimization were 10^{-4} a.u. on energy differences and 10^{-3} a.u. on the maximum atomic-force components, respectively. The electronic energies were in all cases converged to 10^{-6} a.u. (atomic coordinates upon reasonable request).

4. Results and discussion

It is worthwhile asking, first, about the changes in the geometry with respect to the first optimization, Fig. 4(b). One can see differences with the initial configuration, where the largest variations are in the S–S distance of two adjacent DD molecules, *ca.* 15%, with the rest of magnitudes changing less than 10%. With respect to the electronic study, we have focused our attention on several key quantities that describe the general properties of the proposed perovskite: the DOS, the BS (plots that will serve to obtain the gap), the VB and CB, and the changes in the electronic clouds.

The DOS can be found in Fig. 5(a), in which the intermediate value for the corresponding gap, 2.55 eV, reveals the semiconductor character of the material (E_F = 1.87 eV). It is clearly seen the contribution of the iodine atom in the VB and the molecule in the CB, Fig. 5(b). This behaviour is similar to that found in ref. 33 for n = 3 and 4, but it is different from other similar systems, where the first contribution to the CB comes from the inorganic layer, in particular, the lead.[67] Moreover, this is consistent with the fact that the highest levels of the VB are mainly located in the $[PbI_4]^{2-}$ layers, while the lowest levels of the CB are placed in the DD planes, Fig. 5(e) and (f), respectively (only one state shown). For ease of comparison, the structure of the PbI4DD perovskite is included in Fig. 5(c). As a result of the highly significant role played by the DD molecule in the CB, a substantial change occurs in its electronic structure, Fig. 5(d), where the charge density minus the charge density of the

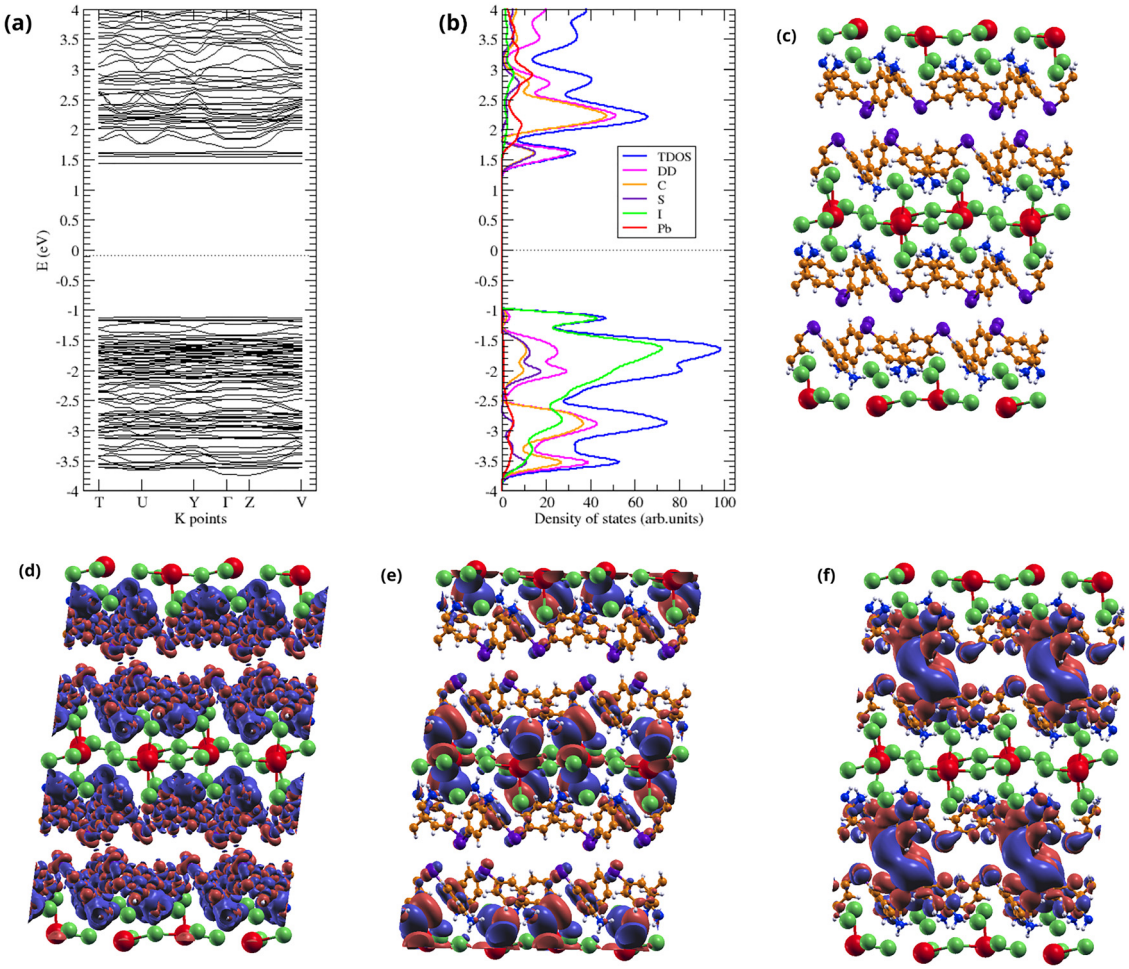

Fig. 5 Band structures and total density of states for the perovskite form proposed here, panels (a) and (b), shifted by E_F. It is clearly seen the contribution of the iodine atom in the valence band and the 4,4′-dithiodianiline molecule in the conduction band, in which the carbon and sulfur atoms play the most important role. The partial profile of the lead is also included and a gap of 2.55 eV is found. As a reference for the rest of the panels, the PbI4DD structure is included in panel (c) and the change in the charge density with respect to the isolated atomic species can be seen in panel (d). In the highest level of the valence band, panel (e), the main contribution comes from the $[PbI_4]^{2-}$ layers, while in the lowest level of the conduction band, panel (f), that contribution is due to the sheets of the 4,4′-dithiodianiline spacer. Colour code as in Fig. 1.

isolated atomic species is plotted. It can be observed that the largest differences are located on the organic framework and it is reasonable if one takes into account that the carbon, hydrogen, nitrogen and sulfur atoms have a much smaller volume than the lead and iodine atoms, being therefore more easily susceptible to changes in their electron clouds.

Having established the main contribution of the DD molecule to the CB, the presence of the carbon atom is to be expected, Fig. 5(b), as it forms the backbone of the organic molecule. However, the appearance of the sulfur atom is noteworthy, Fig. 5(b), raising the question of whether the S atom plays an additional electronic role beyond its mechanical importance in the torsion angle. Taking into account that electrical conductivity arises from the transfer of electrons from the highest levels of the VB to the lowest levels of the CB, it can be inferred from Fig. 5(e) and (f) that, in the present case, conduction occurs from the $[PbI_4]^{2-}$ layers to the DD planes. This suggests that electronic conduction is possible from one inorganic layer to the other through the organic framework, which can be considered as a bridge. Therefore, in this case, the spacer not only has a geometric function but also exerts an electronic influence on the energetic description, at least to the same extent as the inorganic layers. This observation opens the door to exploring species that enable charge transport not only within the inorganic layer of the perovskite, but also in the perpendicular direction, *i.e.*, through the organic framework.

Finally, regarding the stability of the PbI4DD perovskite, we first mention that we did pursue that force- and stress-based relaxations to a very high degree of accuracy, thereby tracking changes into qualitatively different geometries using vdW-DF-cx, Fig. 4. That alone heightens the probability that we thus found a stable geometry. To support this argument, we present two material-stability tests, both of which are illustrated in Fig. 6. We note that the unit cell, shown in Fig. 6(a), forms a (2D-)layered system as we stack such unit cells on top of each other. We also note that there are no expected (or actual) covalent or ionic

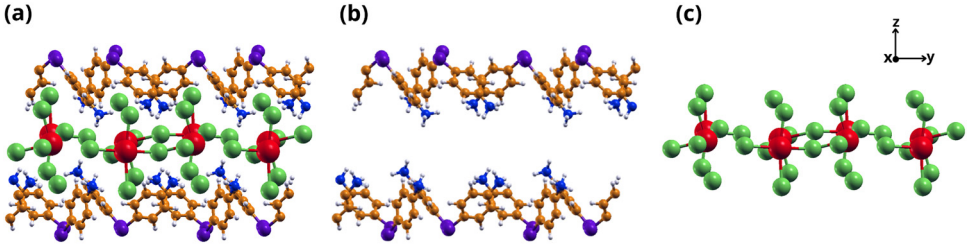

Fig. 6 Perovskite proposed in this work, panel (a), represented as an assembly of PbI_6 octahedra layers, panel (b), and DD planes, panel (c). Colour code as in Fig. 1.

bonding between the top-most set of S atoms in one cell to the set of bottom-most S atoms in the next repeated image.

First, we have used CX to compute the interlayer-binding energy, defined in the typical manner for studies of vdW heterostructures. This was done by increasing the extension of the unit cell in the direction perpendicular to the layer plane by an extra 30 Å, while also tracking what are small relaxations in the increasingly isolated 2D building blocks. We thus predict a 0.85 eV interlayer-binding energy per unit cell, or $\sim$6 meV Å^{-2}, effectively set by the binding contribution ($\sim$9 meV Å^{-2}) from the nonlocal-correlation term, although offset by other energy terms of the CX description. For comparison, the inter-layer binding energy in graphite is $\sim$21 meV Å^{-2}. Second, we computed the energy involved in DD-spacer and PbI-string assembly. That is, we view the unit-cell structure, Fig. 6(a), as arising from an imagined assembly of alternating fragments of DD spacers and $[PbI_4]^{2-}$ layers, Fig. 6(b) and Fig. 6(c), respectively. Here we note that the individual layers (as depicted in the unit cell schematics) results upon charge transfers: the DD molecule, *per se*, has two sulphur-connected aromatic-ring-NH_2 components, whereas the resulting spacer is formed with "NH_3" molecular components, Fig. 6(b), pointing to nearby I atoms, Fig. 6(a) and (c). We find that separating the DD spacer and the $[PbI_4]^{2-}$ layers, *per se*, costs a total of 37 eV per cell (with non-local-correlation binding at 8 eV). However, if the DD spacer were actually thus separated, the system will recover some energy when the 8 N atoms each release one hydrogen atom that, in turn, reattach themselves to surrounding matter. Formation of four H_2 molecules from the DD spacer cluster, Fig. 6(b), is one plausible consequence with significant potential for energy release. We provide an assessment of the energy cost for the would-be material-breakdown path, Fig. 6, by offsetting the 37 eV per cell value by the energy gain involving H detachments and H_2 formation (something we have also tracked in CX studies). The resulting estimate for the energy cost of material disassembly still remains substantial, 21 eV per cell, and we judge the new perovskite system stable.

5. Conclusions

In this work, we have proposed a novel hybrid organic–inorganic bidentate perovskite, PbI4DD, employing diamines as organic spacers, in which the double anchor of the molecule is on the inorganic layer, as for the DJ phases, but the anchoring taking place on the same sheet of octahedra, as for the RP perovskites. Based on our experience we have selected the 4,4′-dithiodianiline diamine as spacer. A first and quick geometric optimization has been performed, repeating the process with a more robust structure optimization, pursued with the Quantum Espresso code, always within the framework of the Density Functional Theory. We have employed the consistent-exchange vdW-DF-cx functional, supplementing in this way the more simple PBEsol calculation, to obtain an accurate description of both the internal structure and inter-molecular excitations. The total density of states, band structure, valence and conduction band, and changes in the electronic clouds, have been obtained, magnitudes which allow us to arrive to the following conclusions:

1. The gap of this new perovskite is equal to 2.55 eV, revealing its semiconductor character.

2. In the valence band the most important contribution comes from the iodine atoms of the PbI_6 octahedra, while in the conduction band the first contributions come from the spacer, specifically, from the carbon and sulfur atoms. It is explained in terms of the location of the highest levels of the VB and the lowest levels of the CB: the former in the inorganic layer, the latter in the organic plane.

3. Therefore, a charge transport in the perpendicular direction of the inorganic layer, *i.e.*, through the spacer, which would act as bridge, is revealed.

These findings open up new possibilities for designing spacers that allow the conduction both in the inorganic layer of the perovskite and in the perpendicular direction, contributing in the quest of new and promising materials in photovoltaics and optoelectronics, for example. Future work may include the experimental validation of the PbI4DD perovskite, as well as further numerical studies on new hybrid organic–inorganic bidentate phases, following the approach adopted in this work.

Author contributions

Conceptualization: Luis Camacho and David López-Durán. Data curation: David López-Durán. Formal analysis: Per Hyldgaard, Luis Camacho and David López-Durán. Funding acquisition: Per Hyldgaard, Gustavo de Miguel, Luis Camacho and David López-Durán. Investigation: Sergio Romero-García, Susana Ramos-Terrón, Gustavo de Miguel, Per Hyldgaard, Luis Camacho and David López-Durán. Methodology: Gustavo de

Miguel, Per Hyldgaard, Luis Camacho and David López-Durán. Resources: Gustavo de Miguel, Per Hyldgaard, Luis Camacho and David López-Durán. Supervision: Per Hyldgaard, Luis Camacho and David López-Durán. Validation: Per Hyldgaard, Luis Camacho and David López-Durán. Visualization: Sergio Romero-García, Luis Camacho, Per Hyldgaard, Susana Ramos Terrón and David López-Durán. Writing - original draft: Per Hyldgaard, Luis Camacho and David López-Durán. Writing - review & editing: Per Hyldgaard, Luis Camacho and David López-Durán.

Conflicts of interest

There are no conflicts to declare.

Data availability

The code employed in this article is Quantum Espresso and can be found at https://www.quantum-espresso.org/ Its references are:

P. Giannozzi, S. Baroni, N. Bonini *et al.*, J. Phys.: Condens. Matter 21 (39), 395502 (2009). DOI: 10.1088/0953-8984/21/39/395502.

P. Giannozzi, O. Andreussi, T. Brumme *et al.*, J. Phys.: Condens. Matter 29 (46), 465901 (2017). DOI: 10.1088/1361-648X/aa8f79.

The version of the code employed for this study is version 6.8.

Acknowledgements

The authors acknowledge funding from the Ministry of Economic Transformation, Industry, Knowledge and Universities (Project Number PY20-00146, Andalusia, Spain), the University of Córdoba (UCO, Institutional Research Plan), the European Union project SUNREY (Contract Number HE-RIA-2021-CL5-D3-101084422), the Swedish Research Foundation (Grant Number 2022-03277), and the Chalmers University of Technology Areas of Advance ''Production'' and ''Nano''. We have carried out the calculations at the servers of the FQM-378 group in the UCO, the facilities of the Scientific Computer Centre of Andalusia, Spain, and at National Academic Infrastructure for Supercomputing in Sweden (NAISS), under contracts NAISS2023-3-22 and NAISS2024-3-16; to whom staff we are very grateful. The figures of this article have been generated with Biovia/Materials Studio,[39] Grace,[68] and XCrysDen.[69]

References

1 J. Sun, J. Wu, X. Tong, F. Lin, Y. Wang and Z. M. Wang, Organic/Inorganic Metal Halide Perovskite Optoelectronic Devices beyond Solar Cells, *Adv. Sci.*, 2018, **5**(5), 1700780.

2 S. D. Stranks and H. J. Snaith, Metal-halide perovskites for photovoltaic and light-emitting devices, *Nat. Nanotechnol.*, 2015, **10**(5), 391.

3 A. Kojima, K. Teshima and Y. Shirai, *et al.*, Organometal Halide Perovskites as Visible-Light Sensitizers for Photovoltaic Cells, *J. Am. Chem. Soc.*, 2009, **131**(17), 6050.

4 S. D. Stranks, G. E. Eperon and G. Grancin, *et al.*, Electron-Hole Diffusion Lengths Exceeding 1 Micrometer in an Organometal Trihalide Perovskite Absorber, *Science*, 2013, **342**, 341.

5 G. C. Xing, N. Mathews and S. Y. Sun, *et al.*, Long-range balanced electron- and hole-transport lengths in organic-inorganic $CH_3NH_3PbI_3$, *Science*, 2013, **342**, 344.

6 C. Motta, F. El-Mellouhi and S. Kais, *et al.*, Revealing the role of organic cations in hybrid halide perovskite $CH_3NH_3PbI_3$, *Nat. Commun.*, 2015, **6**, 7026.

7 G. D. Niu, X. D. Guo and L. D. Wang, Review of recent progress in chemical stability of perovskite solar cells, *J. Mater. Chem. A*, 2015, **3**(17), 8970.

8 C. Eames, J. M. Frost and P. R. F. Barnes, *et al.*, Ionic transport in hybrid lead iodide perovskite solar cells, *Nat. Commun.*, 2015, **6**, 7497.

9 Y. A. Lao, S. Yang and W. J. Yu, *et al.*, Multifunctional π-Conjugated Additives for Halide Perovskite, *Adv. Sci.*, 2022, **9**(17), 2105307.

10 S. Ramos-Terrón, L. Camacho and J. P. Correa-Baena, *et al.*, Chelating diamine surface modifier enhances performance and stability of lead halide perovskite solar cells, *Mater. Today*, 2025, **85**, 60.

11 C. Lin, Y. Tang and Z. Nian, *et al.*, Intralayer bidentate diammoniums for stable two-dimensional perovskites, *Nat. Chem.*, 2026, **18**(2), 275.

12 L. He and Y. Zhou, 2D perovskites featuring intralayer bidentate ligands, *Nat. Chem.*, 2026, **18**(2), 221.

13 P. Hohenberg and W. Kohn, Inhomogeneous Electron Gas, *Phys. Rev. B*, 1964, **136**(3B), B864.

14 W. Kohn and L. J. Sham, Self-Consistent Equations Including Exchange and Correlation Effects, *Phys. Rev.*, 1965, **140**(4A), 1133.

15 K. Berland and P. Hyldgaard, Exchange functional that tests the robustness of the plasmon description of the van der Waals density functional, *Phys. Rev. B:Condens. Matter Mater. Phys.*, 2014, **89**(3), 035412.

16 M. Dion, H. Rydberg and E. Schröder, *et al.*, van der Waals Density Functional for General Geometries, *Phys. Rev. Lett.*, 2004, **92**(24), 246401.

17 T. Thonhauser, V. R. Cooper and S. Li, *et al.*, Van der Waals density functional: Self-consistent potential and the nature of the van der Waals bond, *Phys. Rev. B: Condens. Matter Mater. Phys.*, 2007, **76**(12), 125112.

18 K. Berland, V. R. Cooper and K. Lee, *et al.*, van der Waals forces in density functional theory: a review of the vdW-DF method, *Rep. Prog. Phys.*, 2015, **78**(6), 066501.

19 J. Gong, M. W. Hao and Y. L. Zhang, *et al.*, Layered 2D Halide Perovskites beyond the Ruddlesden–Popper Phase: Tailored Interlayer Chemistries for High-Performance Solar Cells, *Angew. Chem. Int. Ed.*, 2022, **61**(10), e202112022.

20 X. T. Li, J. M. Hoffman and M. G. Kanatzidis, The 2D halide perovskite rulebook: how the spacer influences everything

from the structure to optoelectronic device efficiency, *Chem. Rev.*, 2021, **121**(4), 2230.
21 J. V. Milic, S. M. Zakeeruddin and M. Gratzel, Layered Hybrid Formamidinium Lead Iodide Perovskites: Challenges and Opportunities, *Acc. Chem. Res.*, 2021, **54**(12), 2729.
22 Z. Y. Xu, D. Lu and X. Y. Dong, *et al.*, Highly Efficient and Stable Dion−Jacobson Perovskite Solar Cells Enabled by Extended π-Conjugation of Organic Spacer, *Adv. Mater.*, 2021, **33**(51), 2105083.
23 Q. L. Cao, P. W. Li and W. Chen, *et al.*, Two-dimensional perovskites: Impacts of species, components, and properties of organic spacers on solar cells, *Nano Today*, 2022, **43**, 101394.
24 Y. Gao and X. Dong, and Yongsheng Liu, Recent Progress of Layered Perovskite Solar Cells Incorporating Aromatic Spacers, *Nano-Micro Lett.*, 2023, **15**(1), 169.
25 Z. Y. Lin, J. A. Sun and S. B. Shiring, *et al.*, Design Rules for Two-Dimensional Organic Semiconductor-Incorporated Perovskites (OSiP) Gleaned from Thousands of Simulated Structures, *Angew. Chem., Int. Ed.*, 2023, **62**(33), e202305298.
26 R. Liu, X. Hu and M. X. Xu, *et al.*, Layered Low-Dimensional Ruddlesden-Popper and Dion-Jacobson Perovskites: From Material Properties to Photovoltaic Device Performance, *ChemSusChem*, 2023, **16**(19), e202300736.
27 Z. P. Miao, Q. L. Cao and S. H. Peng, *et al.*, The Spacer Cation with Disulfide Bond for Efficient and Stable Low-Dimensional Dion–Jacobson Perovskite Solar Cells, *Adv. Funct. Mater.*, 2024, **34**(4), 2311135.
28 O. J. Weber, K. L. Marshall and L. M. Dyson, *et al.*, Structural diversity in hybrid organic-inorganic lead iodide materials, *Acta Cryst. B*, 2015, **71**, 668.
29 G. García-Espejo, D. Rodríguez-Padrón and M. Pérez-Morales, *et al.*, Mechanochemical synthesis of one-dimensional (1D) hybrid perovskites incorporating polycyclic aromatic spacers: highly fluorescent cation-based materials, *J. Mater. Chem. C*, 2018, **6**(28), 7677.
30 C. Y. Yue, H. X. Sun and Q. X. Liu, *et al.*, Organic cation directed hybrid lead halides of zero-dimensional to two-dimensional structures with tunable photoluminescence properties, *Inorg. Chem. Front.*, 2019, **6**(10), 2709.
31 Q. Q. Jia, Q. F. Luo and H. F. Ni, *et al.*, High-Sensitivity Organic–Inorganic Hybrid Materials with Reversible Thermochromic Property and Dielectric Switching, *J. Phys. Chem. C*, 2022, **126**(3), 1552.
32 Z. Y. Xu, D. Lu and F. Liu, *et al.*, Phase Distribution and Carrier Dynamics in Multiple-Ring Aromatic Spacer-Based Two-Dimensional Ruddlesden–Popper Perovskite Solar Cells, *ACS Nano*, 2020, **14**(4), 4871.
33 C. Liu, Z. Fang and J. S. Sun, *et al.*, Donor-acceptor-donor type organic spacer for regulating the quantum wells of Dion-Jacobson 2D perovskites, *Nano Energy*, 2022, **93**, 106800.
34 J. Yang, T. W. He and M. Li, *et al.*, π-Conjugated carbazole cations enable wet-stable quasi-2D perovskite photovoltaics, *ACS Energy Lett.*, 2022, **7**(12), 4451.
35 P. Gao, A. B. Yusoff and M. K. Nazeeruddin, Dimensionality engineering of hybrid halide perovskite light absorbers, *Nat. Commun.*, 2018, **9**, 5028.
36 A. H. Coffey, S. J. Yang and M. Gómez, *et al.*, Controlling Crystallization of Quasi-2D Perovskite Solar Cells: Incorporating Bulky Conjugated Ligands, *Adv. Energy Mater.*, 2023, **13**(33), 2201501.
37 C. Zhou, Y. L. Han and L. Cheng, *et al.*, Favorable morphology and compositional distribution enable efficient and stable quasi-2D Dion–Jacobson perovskite solar cells, *J. Mater. Chem. A*, 2023, **11**(21), 11377.
38 J. J. Vittal and K. S. Anjali, Sinusoidal ribbon waves in the crystal structure of bis(4-aminophenyl)disulfide, *Cryst. Eng.*, 1988, **1**(2), 147.
39 Biovia/Materials Studio (San Diego, CA 92121, USA, 2021).
40 J. P. Perdew, A. Ruzsinszky and G. I. Csonka, *et al.*, Restoring the density-gradient expansion for exchange in solids and surfaces, *Phys. Rev. Lett.*, 2008, **100**(13), 136406.
41 A. Tkatchenko and M. Scheffler, Accurate Molecular van der Waals Interactions from Ground-State Electron Density and Free-Atom Reference Data, *Phys. Rev. Lett.*, 2009, **102**(7), 073005.
42 S. Grimme, J. Antony and S. Ehrlich, *et al.*, A consistent and accurate *ab initio* parametrization of density functional dispersion correction (DFT-D) for the 94 elements H-Pu, *J. Chem. Phys.*, 2010, **132**(15), 154104.
43 L. Goerigk, A. Hansen and C. Bauer, *et al.*, A look at the density functional theory zoo with the advanced GMTKN55 database for general main group thermochemistry, kinetics and noncovalent interactions, *Phys. Chem. Chem. Phys.*, 2017, **19**(48), 32184.
44 T. Umebayashi, K. Asai and T. Kondo, *et al.*, Electronic structures of lead iodide based low-dimensional crystals, *Phys. Rev. B:Condens. Matter Mater. Phys.*, 2003, **67**(15), 155405.
45 I. Borriello, G. Cantele and D. Ninno, *Ab initio* investigation of hybrid organic-inorganic perovskites based on tin halides, *Phys. Rev. B: Condens. Matter Mater. Phys.*, 2008, **77**(23), 235214.
46 F. Chiarella, A. Zappettini and F. Licc, *et al.*, Combined experimental and theoretical investigation of optical, structural, and electronic properties of $CH_3NH_3SnX_3$ thin films (X = Cl, Br), *Phys. Rev. B: Condens. Matter Mater. Phys.*, 2008, **77**(4), 045129.
47 H. Z. Lv, H. W. Gao and Y. Yang, *et al.*, Density functional theory (DFT) investigation on the structure and electronic properties of the cubic perovskite $PbTiO_3$, *Appl. Catal. A-Gen.*, 2011, **404**(1–2), 54.
48 P. Giannozzi, S. Baroni and N. Bonin, *et al.*, Quantum Espresso: a modular and open-source software project for quantum simulations of materials, *J. Phys.: Condens. Matter*, 2009, **21**(39), 395502.
49 P. Giannozzi, O. Andreussi and T. Brumme, *et al.*, Advanced capabilities for materials modelling with Quantum Espresso, *J. Phys.: Condens. Matter*, 2017, **29**(46), 465901.
50 D. C. Langreth and J. P. Perdew, Theory of nonuniform electronic systems. I. Analysis of the gradient approximation and a generalization that works, *Phys. Rev. B: Condens. Matter Mater. Phys.*, 1980, **21**(12), 5469.
51 D. C. Langreth and M. J. Mehl, Easily implementable nonlocal exchange-correlation energy functional, *Phys. Rev. Lett.*, 1981, **47**(6), 446.

52 J. P. Perdew and W. Yue, Accurate and simple density functional for the electronic exchange energy: Generalized gradient approximation, *Phys. Rev. B: Condens. Matter Mater. Phys.*, 1986, **33**(12), 8800.
53 D. C. Langreth and S. H. Vosko, Exact electron-gas response functions at high density, *Phys. Rev. Lett.*, 1987, **59**(4), 497.
54 D. C. Langreth and S. H. Vosko, in *Advances in Quantum Chemistry*, ed. P. O. Löwdin, Academic Press, 1990, p. 175.
55 J. P. Perdew and Y. Wang, Accurate and simple analytic representation of the electron-gas correlation energy, *Phys. Rev. B: Condens. Matter Mater. Phys.*, 1992, **45**, 13244.
56 J. P. Perdew, K. Burke and M. Ernzerhof, Generalized gradient approximation made simple, *Phys. Rev. Lett.*, 1996, **77**(18), 3865.
57 M. Ernzerhof and J. P. Perdew, Generalized gradient approximation to the angle-and system-averaged exchange hole, *J. Chem. Phys.*, 1998, **109**(9), 3313.
58 J. P. Perdew, J. A. Chevary and S. H. Vosko, *et al.*, Atoms, molecules, solids, and surfaces: Applications of the generalized gradient approximation for exchange and correlation, *Phys. Rev. B: Condens. Matter Mater. Phys.*, 1992, **46**(11), 6671.
59 F. Tran, J. Stelzl and P. Blaha, Rungs 1 to 4 of DFT Jacob's ladder: Extensive test on the lattice constant, bulk modulus, and cohesive energy of solids, *J. Chem. Phys.*, 2016, **144**(20), 204120.
60 P. Hyldgaard, Y. Jiao and V. Shukla, Screening nature of the van der Waals density functional method: a review and analysis of the many-body physics foundation, *J. Phys.: Condens. Matter*, 2020, **32**(39), 393001.
61 V. Shukla, Y. Jiao and C. M. Frostenson, *et al.*, vdW-DF-ahcx: a range-separated van der Waals density functional hybrid, *J. Phys.: Condens. Matter*, 2022, **34**(2), 025902.
62 V. Shukla, Y. Jiao and J. H. Lee, *et al.*, Accurate nonempirical range-separated hybrid van der Waals density functional for complex molecular problems, solids, and surfaces, *Phys. Rev. X*, 2022, **12**(4), 041003.
63 K. Berland, C. A. Arter and V. R. Cooper, *et al.*, van der Waals density functionals built upon the electron-gas tradition: Facing the challenge of competing interactions, *J. Chem. Phys.*, 2014, **140**(18), 18a539.
64 D. R. Hamann, M. Schluter and C. Chiang, Norm-conserving pseudopotentials, *Phys. Rev. Lett.*, 1979, **43**(20), 1494.
65 C. M. Frostenson, E. J. Granhed and V. Shukla, *et al.*, Hard and soft materials: putting consistent van der Waals density functionals to work, *Electron. Struct.*, 2022, **4**(1), 014001.
66 G. Makov and M. C. Payne, Periodic boundary conditions in *ab initio* calculations, *Phys. Rev. B: Condens. Matter Mater. Phys.*, 1995, **51**(7), 4014.
67 R. Y. Zhao, R. P. Sabatini and T. Zhu, *et al.*, Rigid conjugated diamine templates for stable Dion–Jacobson-type two-dimensional perovskites, *J. Am. Chem. Soc.*, 2021, **143**(47), 19901.
68 Grace v.5.1.22 (Paul J. Turner and Grace Development Team, 1996–2008).
69 A. Kokalj, XCrySDen—a new program for displaying crystalline structures and electron densities, *J. Mol. Graphics Modelling*, 1999, **17**, 176.